Probabilistic Aircraft Conflict Detection Considering Ensemble Weather Forecast

Eulalia Hernández, Alfonso Valenzuela, and Damián Rivas

Department of Aerospace Engineering
Universidad de Sevilla
41092 Seville, Spain
Email: avalenzuela@us.es

***Abstract*—In this paper, the effects of wind uncertainty on the problem of conflict detection are analyzed. The wind components are modeled as random variables; the wind uncertainty is obtained from weather forecasts. The case of two en-route aircraft flying at constant altitude, constant airspeed, constant course, and subject to the same wind is considered. The conflict is caracterized by several indicators, such as the minimum distance between aircraft, the time to minimum distance, and the conflict probability. The analysis is based on the transformation of random variables, which evolves the wind probability density functions to obtain the probability density functions of the indicators. Numerical results are presented for a given particular scenario with uniformly-distributed winds.**

Keywords - conflict detection; wind uncertainty; ensemble weather forecast; transformation of random variables

I. Introduction

In 2005, the European Commission stated the political vision and high level goals for the Single European Sky and its technological pillar SESAR. Accomplishing the goals of increasing capacity and improving safety requires a paradigm shift in operations through state-of-the-art, innovative technology and research. A promising approach that can improve current prediction and optimisation mechanisms towards meeting these goals is to model, analyse, and manage the uncertainty present in ATM.

The sources of uncertainty that affect the ATM system are very disparate, such as known data but in an inexact way (e.g. aircraft take-off weight) or the prediction of the decisions taken by individuals (pilots, controllers,...). Weather uncertainty is one of the main sources of uncertainty that affect the ATM system, as identified by the ComplexWorld Research Network, see Rivas and Vazquez [1].

The inclusion and analysis of weather uncertainty into ATM-related problems has been addressed by many authors. For instance, Zheng and Zhao [2] developed a statistical model of wind uncertainties and applied it to stochastic trajectory prediction in the case of straight, level flight trajectories at constant airspeed with different guidance laws, which affect the distributions of dispersions of the trajectory attributes. Nilim et al. [3] proposed a dynamic routing strategy for an aircraft that minimizes the expected delay when the aircraft's nominal path may be obstructed by bad weather, obtaining significant improvements when compared with more conservative strategies.

In this paper, a preliminary analysis of the effects of the wind uncertainty on the problem of conflict detection is presented. The study is focused on the cruise phase and considers the wind uncertainty provided by Ensemble Prediction Systems (EPS), an approach to weather forecasting that characterizes and quantifies the uncertainty inherent to the prediction. The use of EPS has proved to be an effective way to quantify weather uncertainties. Gonzalez Arribas et al. [4] generated wind-optimal cruise trajectories using pseudospectral methods and studied the sensitivity of the optimal flight paths to the numerical weather prediction uncertainty. Steiner et al. [5] presented an approach, focused on convective storms, of how high-resolution ensemble weather forecasts may get integrated with automated ATM decision support tools. Rivas et al. [6] analyzed the effects of wind uncertainty on aircraft fuel consumption in the case of cruise flight subject to an average constant wind.

Several efforts have been made in the past to solve the problem of conflict detection under the presence of uncertainty. Paielli and Erzberger [7] estimated the probability of conflict for a pair of aircraft in which the trajectory prediction errors were modeled as normally distributed with a constant variance over the whole time horizon; however, the cross correlation of prediction errors between aircraft were not considered. Prandini et al. [8] developed two probabilistic models for predicting the aircraft position in the mid- and near-term future. In the first model, the tracking errors are described by Normal distributions with variances that grow over time and the maximum instantaneous probability is proposed as a criticality measure; in the second model, the aircraft motion is modeled as a deterministic motion plus a Brownian motion perturbation, and expressions for the probability of conflict were obtained. Hu et al. [9] studied the problem of conflict prediction when a spatial correlation structure is assumed for the wind perturbations; they found that the correlation does affect the values of the probability of conflict and cannot be ignored. All the previous works assume a distribution function for the aircraft position, but none of them analyze how the

wind uncertainty propagates and affects conflict detection.

In this work, a conflict between two aircraft is analyzed, both flying at constant airspeed, constant course and constant altitude. The analysis is based on the transformation of random variables, see for example Hogg and Craig [10]. In this method the wind probability density functions (PDFs) are evolved to obtain the PDFs of conflict indicators, such as the minimum distance between aircraft and the time to the minimum distance. The conflict probability is determined as the probability of the minimum distance to be smaller than a given minimum separation. The effects of the wind statistical parameters on the conflict indicators are analyzed for a given particular scenario. Transformation of random variables is the method used, for example, by Rivas et al. [6] to obtain the aircraft fuel consumption when subject to uncertain wind.

The safety and efficiency of the air traffic may benefit from the inclusion of weather uncertainty in automated conflict detection at all levels: long range (over a time horizon of several hours), mid range (tens of minutes), and short range (seconds to minutes). In the long range, the trajectories may be strategically deconflicted even prior to the take-off of the flights thus improving the robustness of the traffic. In the mid and the short range, decision support tools and safety nets, e.g. Medium Term Conflict Detection (MTCD) and Short Term Conflict Alert (STCA), may notify the conflicts to the air traffic controllers according to their probability of occurrence, thus reducing the number of missed and false alerts. Also, the analysis behind the estimation of conflict probability may be useful for developing optimal conflict-resolution algorithms.

II. Trajectory Prediction Considering Ensemble Weather Forecasts

Ensemble weather forecasting is a prediction technique that allows to estimate the uncertainty in a weather forecast. Today's trend is to use Ensemble Prediction Systems (EPS), which consist on running many times a deterministic model from very slightly different initial conditions [11]. Often, the model physics is also slightly perturbed, and some ensembles use more than one model within the ensemble or the same model but with different combinations of physical parameterization schemes. This technique generates a representative sample of the possible realizations of the potential weather outcome, and the hope is that the spread of the predictions in the ensemble brackets the true weather outcome [5].

Typically, an ensemble forecast is a collection of 10 to 50 forecasts (referred to as members). Cheung et al. [12] review various of them: PEARP, from Météo France, consisting of 35 members; MOGREPS, from the UK Met Office, with 12 members; the European ECMWF, with 51 members; and the multi-model ensemble SUPER, constructed by combining the previous three, forming a 98-member ensemble with the aim of capturing outliers and having a higher degree of confidence in predicting the future atmospheric evolution.

As described in the IMET project [13], there are two approaches for trajectory prediction subject to uncertainty provided by ensemble weather forecasts:

1) Ensemble trajectory prediction, where, for each member of the ensemble, a deterministic trajectory predictor is used, leading to an ensemble of trajectories from which probability distributions can be derived; some type of postprocessing is required.
2) Probabilistic trajectory prediction, where probability distributions of meteorological parameters of interest (such as wind) are obtained from the ensemble forecast and evolved using a probabilistic trajectory predictor, leading to probability distributions of trajectory parameters of interest.

The IMET project follows the first approach, and Rivas et al. [6] and this paper follow the second one. Because the ensemble forecasts are subject to biases and dispersion errors, the main advantage of the second approach over the first one is that the probability distributions can be obtained from statistical postprocessing techniques as those described by Gneiting [14]. The aim of these techniques is to improve the quality of the numerical weather forecasts by generating calibrated and sharp probability density functions.

The meteorological parameters considered in this work are the meridional (South-North), w_x, and the zonal (West-East), w_y, components of the wind. The approach to obtain the probability distributions of the wind components is as follows. Suppose that the ensemble has n members, then the first step is to obtain for each wind component and for a given location the n sample values $\{w_{x,1}, ..., w_{x,n}\}$ and $\{w_{y,1}, ..., w_{y,n}\}$. Next, one must assume that each wind component follows a particular distribution. This is not a minor point, and in fact is one of the open challenges in this problem. For example, according to Gneiting [14], each wind component can be approximated by a normal distribution. Finally, the parameters of the chosen distribution are to be estimated from the sample.

Although the formulation presented in this paper is applicable to any probability distribution, for the sake of simplicity the results shown in Section V are obtained for uniform distributions.

III. Conflict Detection

In this work, the following assumptions are considered (see Fig. 1):

- a North-East reference system fixed to Earth is used (x-axis pointing North and y-axis pointing East);
- two aircraft, A and B, fly in the same airspace and are affected by the same wind;
- the wind ($\vec{w}$) is described by its meridional and zonal components (w_x and w_y, respectively), which are uncertain and statistically independent;
- both aircraft fly at constant airspeed (V_A and V_B), constant course (ψ_A and ψ_B), and the same constant altitude;
- the initial positions of both aircraft ($\vec{s}_{0,A}$ and $\vec{s}_{0,B}$), their airspeeds and their courses are perfectly known; and
- the initial separation between the aircraft is greater than a given horizontal separation requirement D (e.g., 5 NM) and they are approaching.

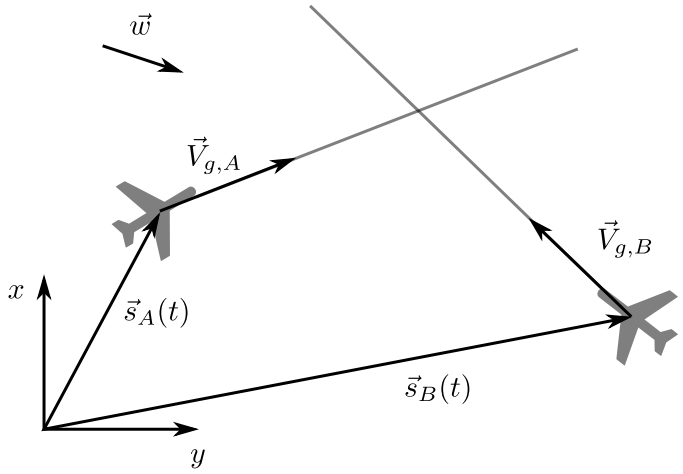

Figure 1. General scenario.

The positions of aircraft A and B at any time t, $\vec{s}_A(t)$ and $\vec{s}_B(t)$, are given by

$$\begin{aligned}\vec{s}_A(t) &= \vec{s}_{0.A} + \vec{V}_{g,A}t,\\ \vec{s}_B(t) &= \vec{s}_{0,B} + \vec{V}_{g,B}t,\end{aligned} \tag{1}$$

where $\vec{V}_{g,A}$ and $\vec{V}_{g,B}$ are their ground speeds. Since the airspeeds and courses are perfectly known but the wind is uncertain, the aircraft headings and the magnitudes of the ground speeds $\vec{V}_{g,A}$ and $\vec{V}_{g,B}$ are uncertain. The ground speeds can be obtained from the wind triangles (see Fig. 2):

$$\begin{aligned}\vec{V}_{g,A} &= \vec{V}_A + \vec{w}\\ &= V_A \begin{bmatrix}\cos\left(\psi_A - \arcsin\left(\frac{w_{c,A}}{V_A}\right)\right)\\ \sin\left(\psi_A - \arcsin\left(\frac{w_{c,A}}{V_A}\right)\right)\end{bmatrix} + \begin{bmatrix}w_x\\ w_y\end{bmatrix},\end{aligned} \tag{2}$$

$$\begin{aligned}\vec{V}_{g,B} &= \vec{V}_B + \vec{w}\\ &= V_B \begin{bmatrix}\cos\left(\psi_B - \arcsin\left(\frac{w_{c,B}}{V_B}\right)\right)\\ \sin\left(\psi_B - \arcsin\left(\frac{w_{c,B}}{V_B}\right)\right)\end{bmatrix} + \begin{bmatrix}w_x\\ w_y\end{bmatrix},\end{aligned} \tag{3}$$

where $w_{c,A}$ and $w_{c,B}$ are the crosswinds affecting aircraft A and B, respectively. In these expressions, it has been considered that crosswinds are positive if they are from the left wing; they are given by

$$\begin{aligned}w_{c,A} &= w_y \cos\psi_A - w_x \sin\psi_A,\\ w_{c,B} &= w_y \cos\psi_B - w_x \sin\psi_B.\end{aligned} \tag{4}$$

As it will be seen below, the indicators chosen in this work to characterize the conflict only depend on the relative motion between the two aircraft. The relative position between them, $\vec{s}(t) = \vec{s}_B(t) - \vec{s}_A(t)$, can be written as (from (1))

$$\vec{s}(t) = \vec{s}_0 + \vec{V}_g t, \tag{5}$$

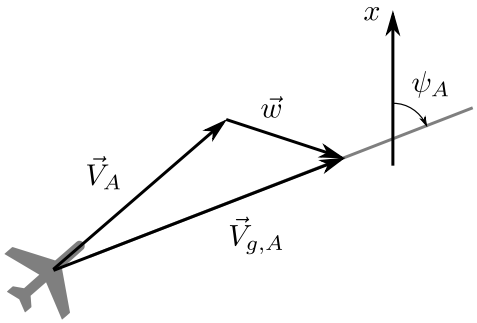

Figure 2. Wind triangle for aircraft A.

where the relative initial position, $\vec{s}_0$, and the relative ground speed, $\vec{V}_g$, are given by

$$\begin{aligned}\vec{s}_0 &= \vec{s}_{0,B} - \vec{s}_{0,A},\\ \vec{V}_g &= \vec{V}_{g,B} - \vec{V}_{g,A}.\end{aligned} \tag{6}$$

Substituting Eqns. (2) and (3) into the relative ground speed one obtains

$$\begin{aligned}\vec{V}_g =& V_B \begin{bmatrix}\cos\left(\psi_B - \arcsin\left(\frac{w_{c,B}}{V_B}\right)\right)\\ \sin\left(\psi_B - \arcsin\left(\frac{w_{c,B}}{V_B}\right)\right)\end{bmatrix}\\ &- V_A \begin{bmatrix}\cos\left(\psi_A - \arcsin\left(\frac{w_{c,A}}{V_A}\right)\right)\\ \sin\left(\psi_A - \arcsin\left(\frac{w_{c,A}}{V_A}\right)\right)\end{bmatrix}.\end{aligned} \tag{7}$$

Notice that $\vec{s}_0$ is certain because both initial positions $\vec{s}_{0,A}$ an $\vec{s}_{0,B}$ are perfectly known; however, $\vec{V}_g$ is uncertain (in magnitude and direction) because of the wind. It is important to notice that $\vec{V}_g$ is affected by the crosswinds but not by the along-track winds.

The distance between the two aircraft at any time, $d(t)$, is the magnitude of the relative position, $d(t) = \|\vec{s}(t)\|$. In terms of $\vec{s}_0$ and $\vec{V}_g$, it can be expressed as

$$d(t) = \sqrt{s_0^2 + 2\vec{s}_0\vec{V}_g t + V_g^2 t^2}. \tag{8}$$

The minimum distance between the two aircraft, d_{min}, is then given by

$$d_{min} = \sqrt{s_0^2 - \frac{\left(\vec{s}_0\vec{V}_g\right)^2}{V_g^2}}. \tag{9}$$

A conflict exists if a given set of separation minima is predicted to be violated; in this work, since it is assumed that the aircraft are flying at the same altitude and they are approaching, a conflict exists if the minimum distance d_{min} is found to be smaller than the separation requirement D: $d_{min} \leq D$. The presence of uncertainty in $\vec{V}_g$ makes $d(t)$ and d_{min} to be uncertain, and therefore the existence of a conflict is also uncertain. Next, several indicators are defined to characterize the conflict.

- **Minimum distance, d_{min}.**
  The minimum distance between the two aircraft can be seen as an indicator of the conflict intensity. It is given by (9).
- **Time to minimum distance, $t_{d_{min}}$.**
  Since it is assumed that the aircraft are approaching, the minimum distance will always be found at $t > 0$. The time instant at which the minimum separation takes place, $t_{d_{min}}$, is given by

$$t_{d_{min}} = \frac{-\vec{s}_0 \vec{V}_g}{V_g^2}. \tag{10}$$

- **Probability of conflict, P_{con}.**
  The probability of the existence of a conflict, P_{con}, is given by the probability of d_{min} being smaller than D

$$P_{con} = P[d_{min} \leq D]. \tag{11}$$

Notice that all these conflict indicators depend on the crosswinds through $\vec{V}_g$ but not on the along-track winds; however, the motion of each aircraft does depend on the along-track winds. A particular case of interest can be highlighted: when the two aircraft fly at opposite courses and the wind is aligned with the courses. In this case, both crosswinds are nil, $w_{c,A} = w_{c,B} = 0$, and $\vec{V}_g$ results to be certain. Therefore, the relative motion is certain but the position of each aircraft is uncertain because $\vec{V}_{g,A}$ and $\vec{V}_{g,B}$ are uncertain due to the along-track winds. This is a clear example of how the wind uncertainty affects the trajectory of each aircraft without affecting some traffic properties; that is, the uncertainty at the trajectory scale (microscale) does not propagate to the traffic scale (mesoscale).

IV. Transformation of Random Variables

The PDFs of the conflict indicators described in Section III are obtained using a bivariate transformation of random variables. The basis of this transformation is as follows [10]: Let u_1 and u_2 be two random variables having joint PDF $f_{u_1,u_2}(u_1, u_2)$, and let R_{u_1,u_2} be the two-dimensional set in the u_1u_2-plane where $f_{u_1,u_2}(u_1, u_2) > 0$. Let v_1 and v_2 be two random variables whose PDFs are to be found. Let $v_1 = g_1(u_1, u_2)$ and $v_2 = g_2(u_1, u_2)$ define a one-to-one transformation of R_{u_1,u_2} onto a set R_{v_1,v_2} in the v_1v_2-plane. If u_1 and u_2 are expressed in terms of v_1 and v_2, one can write $u_1 = h_1(v_1, v_2)$ and $u_2 = h_2(v_1, v_2)$. Then, the joint PDF of v_1 and v_2 is given by

$$f_{v_1,v_2}(v_1, v_2) = f_{u_1,u_2}(h_1(v_1, v_2), h_2(v_1, v_2))\,|J| \tag{12}$$

if $(v_1, v_2) \in R_{v_1,v_2}$, and 0 otherwise. $|J|$ is the absolute value of the Jacobian determinant

$$J = \begin{vmatrix} \dfrac{\partial h_1(v_1,v_2)}{\partial v_1} & \dfrac{\partial h_1(v_1,v_2)}{\partial v_2} \\ \dfrac{\partial h_2(v_1,v_2)}{\partial v_1} & \dfrac{\partial h_2(v_1,v_2)}{\partial v_2} \end{vmatrix}. \tag{13}$$

In case that $g_1(u_1, u_2)$ and $g_2(u_1, u_2)$ define a more-to-one transformation, then it is necessary to separate the transformation into disjoint regions where the transformation is one-to-one.

The marginal PDF of v_1, $f_{v_1}(v_1)$, can be obtained from the joint PDF $f_{v_1,v_2}(v_1, v_2)$ by integrating in v_2

$$f_{v_1}(v_1) = \int_{-\infty}^{\infty} f_{v_1,v_2}(v_1, v_2)\mathrm{d}v_2. \tag{14}$$

Once the PDF $f_{v_1}(v_1)$ is known, one can compute the mean, the typical deviation, and the probability of v_1 being smaller than a given value a as follows

$$\begin{aligned} E[v_1] &= \int_{-\infty}^{\infty} v_1 f_{v_1}(v_1)\mathrm{d}v_1, \\ \sigma[v_1] &= \left[\int_{-\infty}^{\infty} v_1^2 f_{v_1}(v_1)\mathrm{d}v_1 - (E[v_1])^2\right]^{1/2}, \\ P[v_1 < a] &= \int_{-\infty}^{a} f_{v_1}(v_1)\mathrm{d}v_1. \end{aligned} \tag{15}$$

In this work, the two random variables u_1 and u_2 are the two wind components w_x and w_y; the random variable v_1 is any of the indicators d_{min} or $t_{d_{min}}$; and the random variable v_2 is a dummy variable which, for simplicity, has been chosen to be the wind component w_y.

Since the indicators defined in this problem do not allow to obtain analytical expressions for the inverse transformations $h_1(v_1, v_2)$ and $h_2(v_1, v_2)$, then these inverses, the partial derivatives, and the integrations are computed numerically.

V. Results

In the following, some initial results are presented for a particular scenario and arbitrary winds distributed uniformly. The initial positions, airspeeds and courses of aircraft A and B are the following (see Fig. 3): $\vec{s}_{0,A} = [0, 0]$, $\vec{s}_{0,B} = [18520, 18520]$ m, $V_A = V_B = 240$ m/s, $\psi_A = 90$ deg, and $\psi_B = 135$ deg. The horizontal separation requirement D is set to 5 NM (9260 m).

The wind components w_x and w_y are considered to be independent and both are described by the following PDF

$$f_{w_i}(w_i) = \begin{cases} 1/\left(2\delta_w\right), & w_i \in [\bar{w} - \delta_w, \bar{w} + \delta_w], \\ 0, & \text{otherwise}, \end{cases} \tag{16}$$

where $i \in \{x, y\}$, the mean value of the distribution $\bar{w}$ varies between -20 m/s and 20 m/s, and the half-width δ_w varies between 0 and 25 m/s. For simplicity, it has been decided in this particular application to consider the same PDF for both winds; as a result of this decision, positive values of $\bar{w}$ means that on average the wind points Northeast and negative values of $\bar{w}$ means that on average the wind points Southwest.

Since the two wind components are considered to be statistically independent, the joint PDF of w_x and w_y is the product of the individual PDFs

$$f_{w_x,w_y}(w_x, w_y) = f_{w_x}(w_x) f_{w_y}(w_y). \tag{17}$$

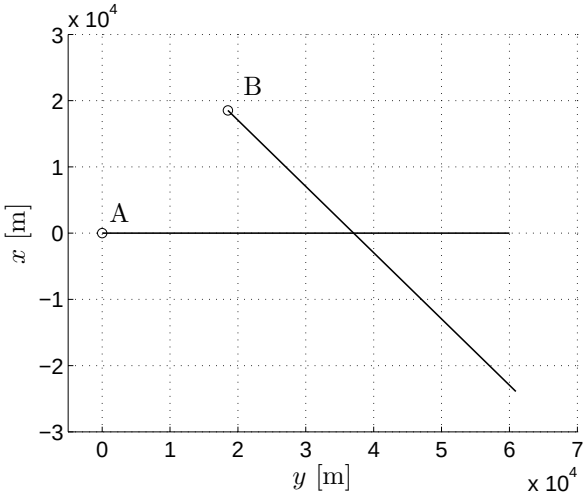

Figure 3. Aircraft trajectories.

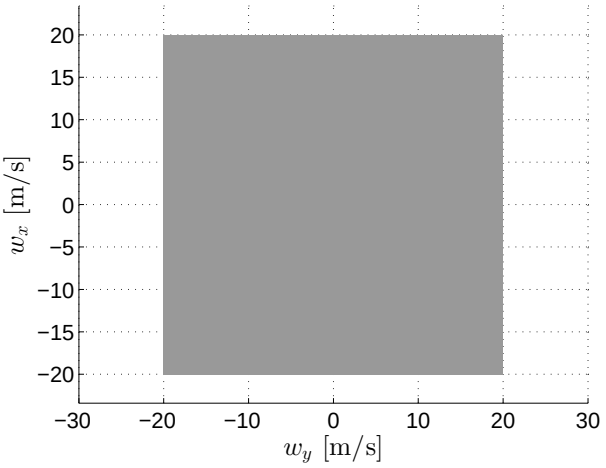

Figure 4. Two-dimensional set in the $w_x w_y$-plane, for $\bar{w} = 0$ and $\delta_w = 20$ m/s.

Next, results are presented for each indicator. All the results are validated by the Monte Carlo method; the number of samples for each simulation (i.e., for each value of $\bar{w}$ and δ_w) is 2^{23} (aprox. 8.4 million). The probability of having an error on the mean value of an indicator obtained by the Monte Carlo method, $\bar{v}_1$, larger than some given tolerance, ε, can be estimated as (see Bayer et al. [15])

$$P[|\bar{v}_1 - E[v_1]| > \varepsilon] \approx 2\left(1 - \Phi\left[\frac{\sqrt{N}\varepsilon}{\sigma[v_1]}\right]\right), \qquad (18)$$

where N is the number of samples and Φ is the standard normal cumulative distribution function. As a reference, for $\bar{w} = 0$, $\delta_w = 20$ m/s, and the chosen number of samples $N = 2^{23}$, the probability of having an error larger than 1 m in the mean value of d_{min} is 0.71%. As it will be seen in all cases, the results obtained with the Monte Carlo method are almost indistinguishable from those obtained with the transformation method.

A. *Minimum distance, d_{min}*

Initially, results are presented for $\bar{w} = 0$ and $\delta_w = 20$ m/s. The two-dimensional set R_{w_x,w_y} and its transformation onto the $d_{min}w_y$-plane, R_{d_{min},w_y}, are presented in Figs. 4 and 5, respectively. The PDF of d_{min} is shown in Fig. 6. The existence of the four corners of the PDF (at 7.5, 9.0, 11.0, and 12.4 km approximately, labeled as c, d, b, and a, respectively) can be explained by the four corners of R_{d_{min},w_y} (labeled with the same letters): when the marginal PDF is obtained by integrating on w_y, these corners represent abrupt changes in the integration limits.

The expected value and the standard deviation of d_{min} are 10012 and 1076 m, respectively (10013 and 1076 m with Monte Carlo method). The probability of conflict is $P_{con} = 28.0\%$, which is obtained as the area under the PDF to the left of the vertical line that represents the separation minimum D (vertical dash-dot line in Fig. 6).

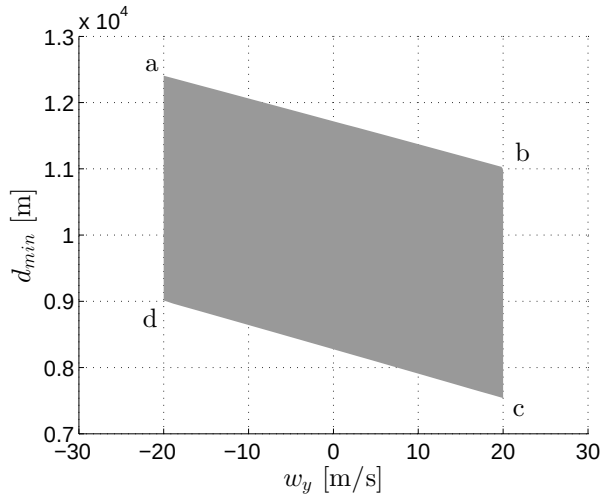

Figure 5. Two-dimensional set in the $d_{min}w_y$-plane, for $\bar{w} = 0$ and $\delta_w = 20$ m/s.

Next, results are presented for different values of the mean wind $\bar{w}$ and the width δ_w. In Fig. 7 it can be seen that the expected value $E[d_{min}]$ does not depend on δ_w and decreases as $\bar{w}$ increases. Since $E[d_{min}]$ does not depend on δ_w, its evolution with $\bar{w}$ can be explained considering the deterministic case (i.e., $\delta_w = 0$): as $\bar{w}$ increases the wind changes from pointing Southwest to pointing Northeast; both airspeeds $\vec{V}_A$ and $\vec{V}_B$ rotate clockwise to keep their course constant, being aircraft B more affected by the wind because the wind direction is entirely perpendicular to its course; as a result, $\vec{V}_g$ also rotates clockwise (see Fig. 8), being more aligned with $\vec{s}_0$; hence, the term $\left(\vec{s}_0\vec{V}_g\right)^2/V_g^2$ increases and thus d_{min} decreases.

The standard deviation $\sigma[d_{min}]$ is shown in Fig. 9. As expected, it increases as δ_w increases; as a numerical reference,

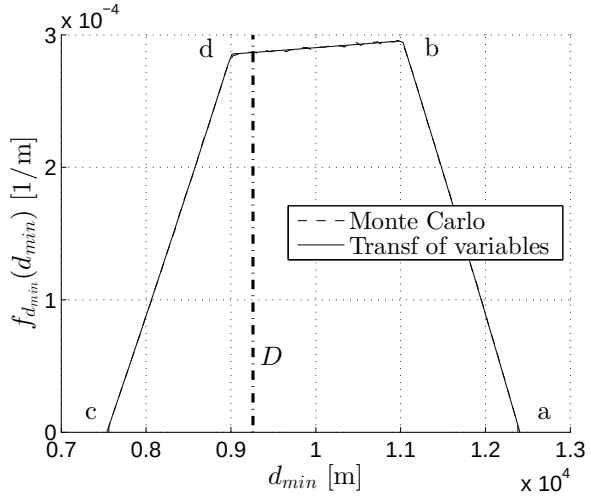

Figure 6. PDF of d_{min}, for $\bar{w} = 0$ and $\delta_w = 20$ m/s.

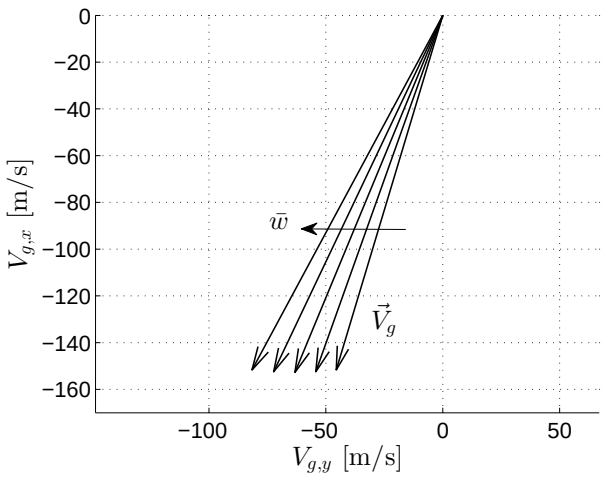

Figure 8. $\vec{V}_g$ for $\bar{w} = -20, -10, 0, 10, 20$ m/s and $\delta_w = 0$.

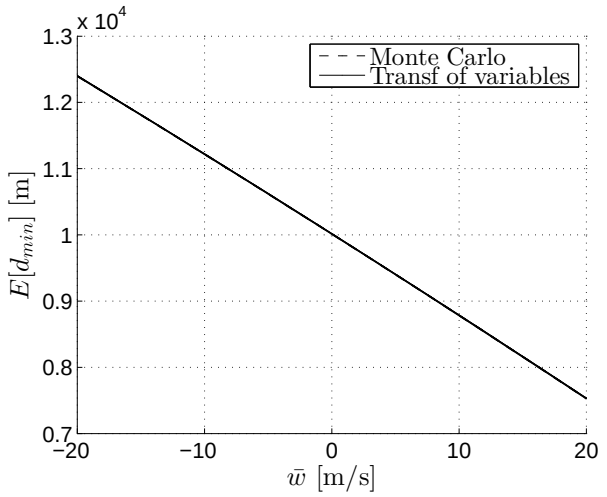

Figure 7. Expected value of d_{min} as a function of $\bar{w}$, for $\delta_w = 5, 10, 15, 20, 25$ m/s.

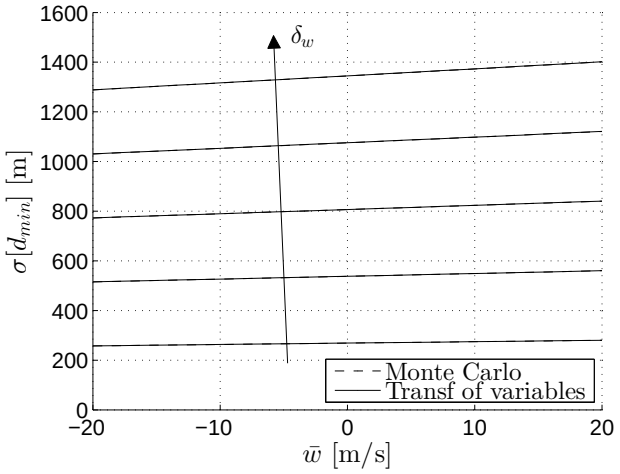

Figure 9. Standard deviation of d_{min} as a function of $\bar{w}$, for $\delta_w = 5, 10, 15, 20, 25$ m/s.

for $\bar{w} = 0$ it increases 54 m when δ_w increases 1 m/s. Its dependence with $\bar{w}$ is very weak, increasing very slightly.

B. Time to minimum distance, $t_{d_{min}}$

The $R_{t_{d_{min}},w_y}$ region and the PDF of $t_{d_{min}}$ are depicted in Figs. 10 and 11, respectively, for $\bar{w} = 0$ and $\delta_w = 20$ m/s. As in the case of d_{min}, the PDF shows four corners, two of them very close to each other (at approximately 130 s) and hard to distinguish; as in the case of d_{min}, the existence of these corners can be explained by the four corners of $R_{t_{d_{min}},w_y}$. The expected value and the standard deviation are 131.9 and 6.4 s, respectively (same values are obtained with Monte Carlo method).

The evolution of the expected value $E[t_{d_{min}}]$ and the standard deviation $\sigma[t_{d_{min}}]$ with the mean wind $\bar{w}$ and the width δ_w is shown in Figs. 12 and 13, respectively. It can be seen that $E[t_{d_{min}}]$ is almost independent of both wind parameters, and that $\sigma[t_{d_{min}}]$ depends very weakly on $\bar{w}$ (it decreases very slightly). As in the case of d_{min}, the evolution of the expected value can be analized considering the deterministic case: as $\bar{w}$ increases $\vec{V}_g$ rotates clockwise and its magnitude also increases (see Fig. 8), the term $\left(\vec{s}_0 \vec{V}_g\right)/V_g^2$ happens to remain approximately constant. Obviously, this result pertains to the particular scenario considered in this paper and cannot be generalized.

As expected, $\sigma[t_{d_{min}}]$ increases as δ_w increases. As a numerical reference, for $\bar{w} = 0$, $\sigma[t_{d_{min}}]$ increases 0.3 s when δ_w increases 1 m/s. Its dependence with $\bar{w}$ is very weak, decreasing very slightly.

C. Probability of conflict, P_{con}

The probability of conflict P_{con} is shown in Fig. 14 for different values of $\bar{w}$ and δ_w. In this figure, the deterministic case has been also included ($\delta_w = 0$) as a reference; it is

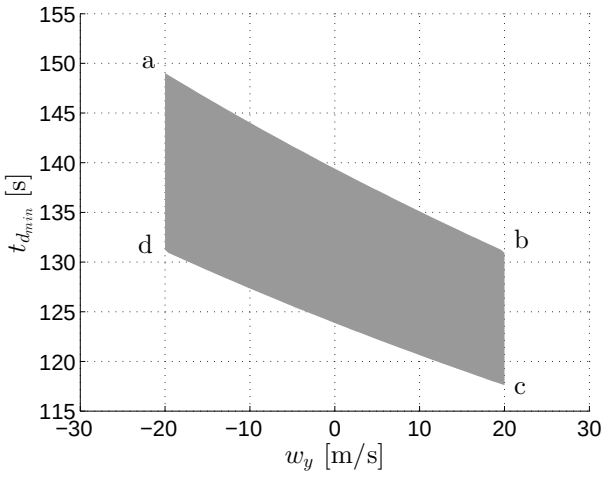

Figure 10. Two-dimensional set in the $t_{d_{min}} w_y$-plane, for $\bar{w} = 0$ and $\delta_w = 20$ m/s.

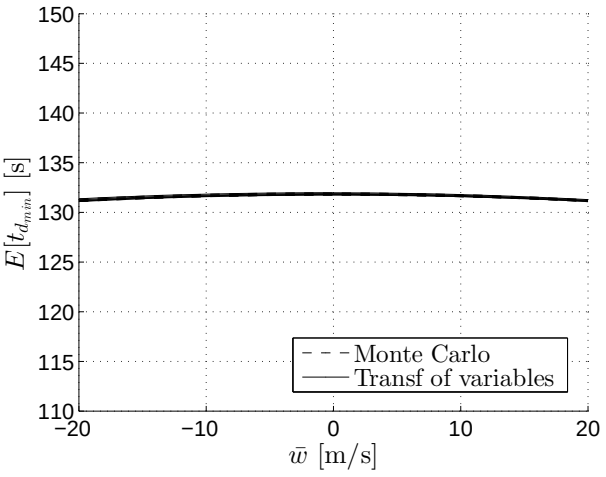

Figure 12. Expected value of $t_{d_{min}}$ as a function of $\bar{w}$, for $\delta_w = 5, 10, 15, 20, 25$ m/s.

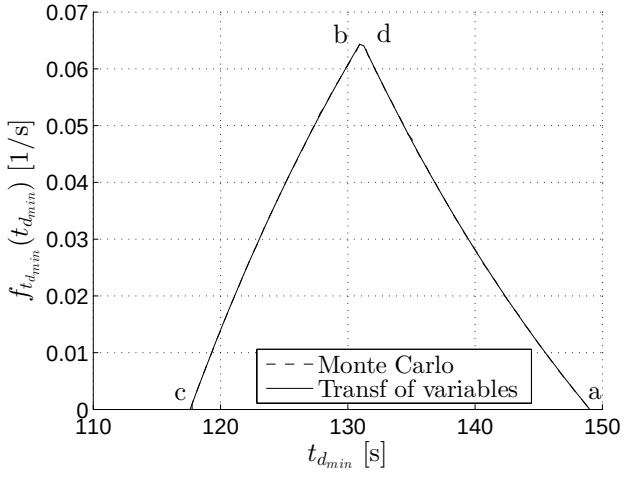

Figure 11. PDF of $t_{d_{min}}$, for $\bar{w} = 0$ and $\delta_w = 20$ m/s.

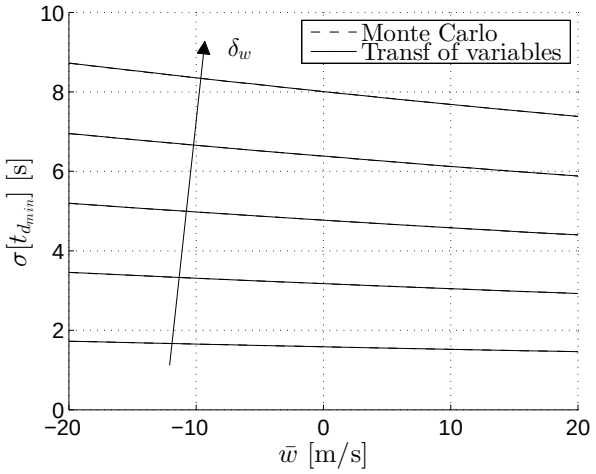

Figure 13. Standard deviation of $t_{d_{min}}$ as a function of $\bar{w}$, for $\delta_w = 5, 10, 15, 20, 25$ m/s.

represented by the line that changes instantly from 0 to 100 % probability at $\bar{w} = 6.2$ m/s. It can be seen that for large negative values of $\bar{w}$ and any value of δ_w the probability is nil ($P_{con} = 0$) because the minimum distance between aircraft is large (see Fig. 7). As $\bar{w}$ increases, P_{con} increases because the minimum distance decreases, and at some point the conflict becomes certain ($P_{con} = 100$ %).

P_{con} can decrease or increase as δ_w increases, depending on the value of $\bar{w}$. In this application, it has been found that, when no conflict exists in the deterministic case ($\bar{w} < 6.2$ m/s), an increase of the wind uncertainty results in a higher probability of having winds which can result into a conflict, thus increasing P_{con}. On the contrary, when a conflict exists in the deterministic case ($\bar{w} > 6.2$ m/s), as the wind uncertainty increases, a higher probability of having winds which do not result into a conflict also increases, thus reducing P_{con}. In both cases, the certainty that a conflict does exist or does not exist decreases as the wind uncertainty increases.

VI. Conclusions

The general framework for this paper is the development of a methodology to manage weather uncertainty suitable to be integrated into the traffic management process. This work is a first step focused on the assessment of the impact of wind uncertainty on conflict detection, and in particular on the en-route phase of flight. The methodology presented in this work allows to assess the probability of conflict in given scenarios and other uncertain characteristics of the conflict. It is expected that by considering the weather uncertainty in the trajectory prediction process, the safety and efficiency of the air traffic may be improved by strategically deconflicting the trajectories and by reducing the number of missed and false alerts.